

## Supporting Information

# Ultrafast growth of submillimeter-scale single-crystal **MoSe<sub>2</sub>** by pre-alloying CVD

Xing Xin,<sup>‡a,b</sup> Jiamei Chen,<sup>‡a</sup> Yanmei Zhang,<sup>a</sup> Mao-Lin Chen,<sup>c</sup> Youzhe Bao,<sup>a</sup> Weizhen Liu,<sup>a</sup> Yichun Liu,<sup>a</sup> Haiyang Xu<sup>\*a</sup> and Wencai Ren<sup>\*b,d</sup>

<sup>a</sup>Centre for Advanced Optoelectronic Functional Materials Research and Key Laboratory of UV-Emitting Materials and Technology, Northeast Normal University, Ministry of Education, Changchun 130024, China.

<sup>b</sup>Shenyang National Laboratory for Materials Science, Institute of Metal Research, Chinese Academy of Science, Shenyang 110016, P. R. China.

<sup>c</sup>State Key Laboratory of Quantum Optics and Quantum Optics Devices, Institute of Optoelectronics, Shanxi University, Taiyuan 03006, China.

<sup>d</sup>School of Material Science and Engineering, University of Science and Technology of China, Shenyang 110016, P. R. China

E-mail: hyxu@nenu.edu.cn, wcren@imr.ac.cn

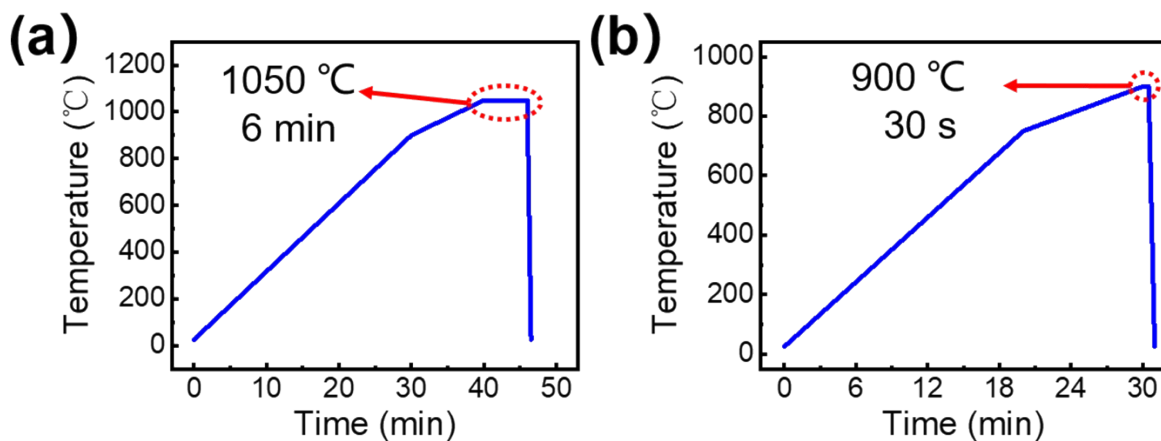


**Figure S1.** Schematic of (a) pre-alloying process for Au foils and (b) CVD process to grow large-scale monolayer MoSe<sub>2</sub> single crystals on pre-alloyed Au foils.

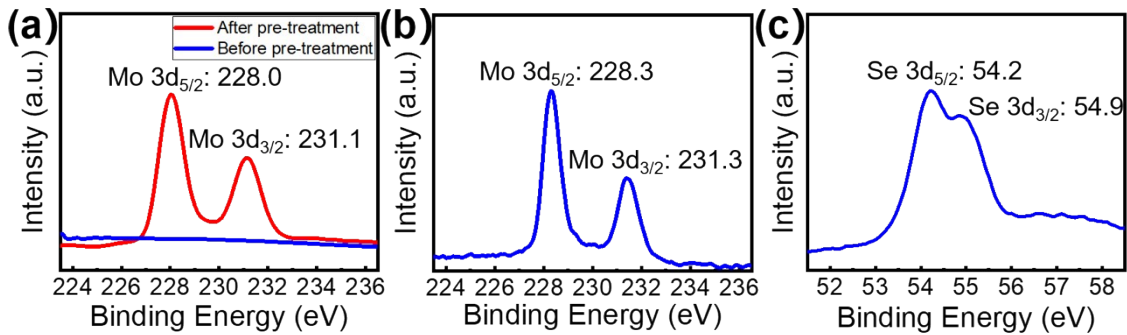


**Figure S2.** XPS spectra of elemental changes on Au foils. (a) The variation of Mo content in Au foils before and after pre-treatment with  $\text{MoO}_3$ . The XPS spectra of (b) Mo and (c) Se in the pre-alloyed Au foils detected after the  $\text{MoSe}_2$  growth.

Au foils were pre-treated by  $\text{H}_2$  reduction of  $\text{MoO}_3$  to form pre-alloyed Au. Figure S2a shows that no Mo peak exists on the Au surface before pre-alloying. After pre-alloying, the peaks of 228.0 eV and 231.1 eV appear, which are consistent with Mo 3d<sub>5/2</sub> and Mo 3d<sub>3/2</sub> peaks, indicating the formation of Au-Mo alloys. Figure S2b and S2c exhibit that Mo 3d<sub>5/2</sub> and 3d<sub>3/2</sub> peaks are located at  $\sim$ 228.3 and 231.3 eV, while Se 3d<sub>5/2</sub> and 3d<sub>3/2</sub> peaks are located at  $\sim$ 54.2 and 54.9 eV, respectively, illustrating the formation of  $\text{MoSe}_2$  on pre-alloyed Au foils. Mo in Au-Mo alloys or  $\text{MoSe}_2$  can be distinguished by the position of Mo peaks in XPS spectra.

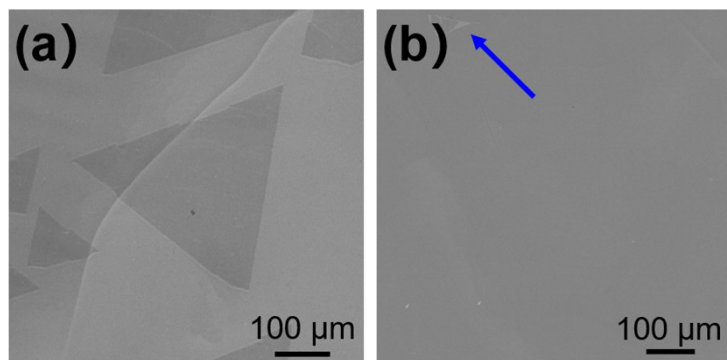


**Figure S3.** The SEM images of  $\text{MoSe}_2$  (a) single crystals and (b) a continuous film. The blue arrow in (b) shows the naked Au area without  $\text{MoSe}_2$ .  $\text{MoSe}_2$  film over a large area represents uniformly monolayer without any multilayer.

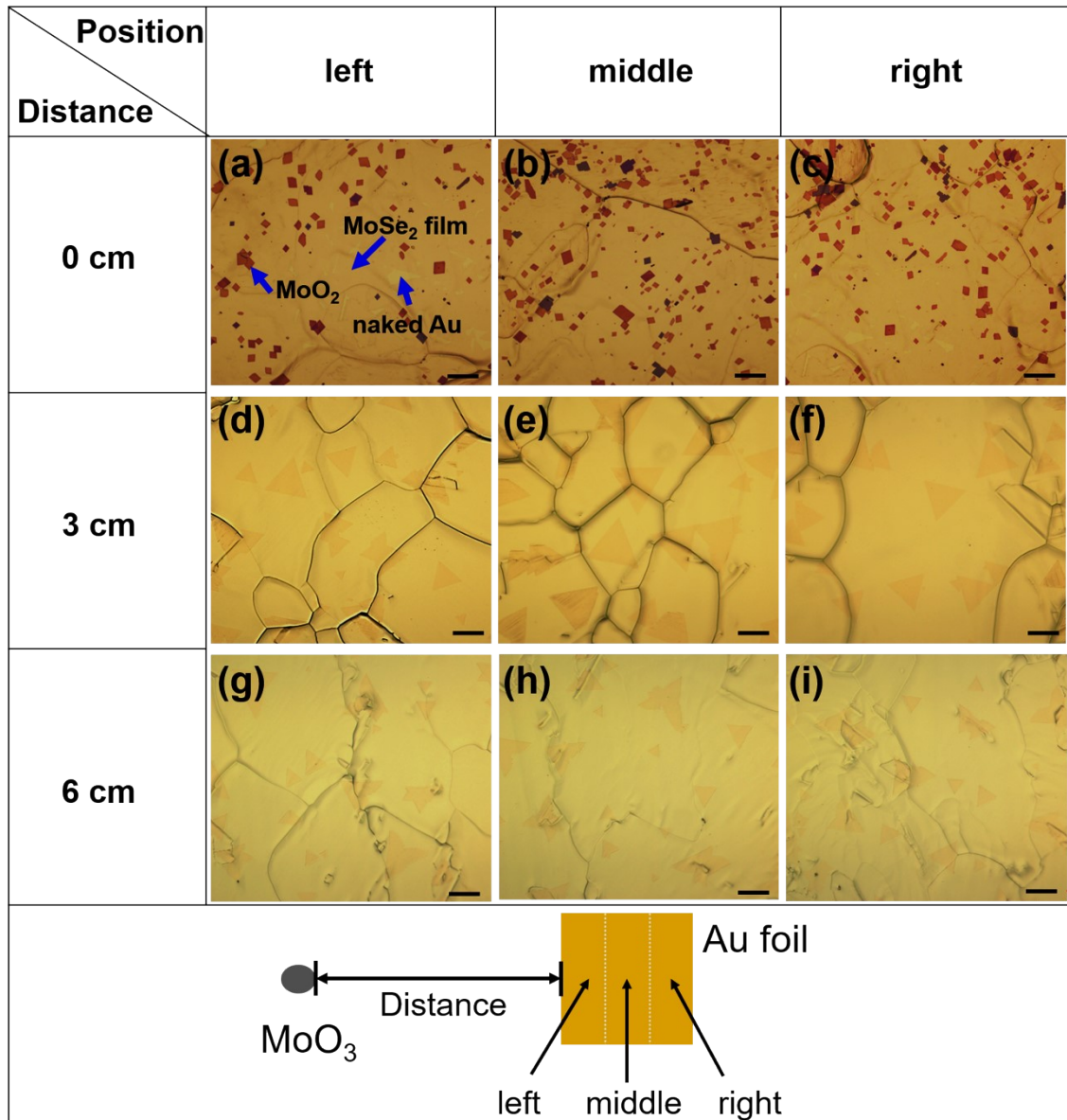


**Figure S4.** Optical images of MoSe<sub>2</sub> grown on the different areas (left, middle, right) of pre-alloyed Au foils with changing the distance (D) between Au foils and MoO<sub>3</sub> powders for (a-c) D = ~0 cm, (d-f) D = ~3 cm, and (g-i) D = ~6 cm. Au foils were pre-alloyed at 1050 °C for 4 times. The scale bars in all images are 100 μm.

We have explored morphology evolution of MoSe<sub>2</sub> with changing the distance (D) between Au foils and MoO<sub>3</sub> powders in Figure S4. When Au foil was very close to MoO<sub>3</sub> (D=0 cm, Figure S4a-c,) MoSe<sub>2</sub> domains join together to form a film and parallelogram-like MoO<sub>2</sub> also appeared. When D was increased to ~3 cm, the individual triangle MoSe<sub>2</sub> single crystals were obtained with the disappearance of MoO<sub>2</sub> flakes (Figure S4d-f). With further increasing D to ~6 cm (Figure S4g-i), MoSe<sub>2</sub> domains become smaller and a little irregular because of the insufficient Mo source supply. The above results indicate that the morphology of MoSe<sub>2</sub> depended on D due to the MoO<sub>3</sub> with point-like distribution.

However, in our experiments, the size of Au foils was 1 cm × 1 cm. When D was fixed at 3 cm, the morphology of MoSe<sub>2</sub> on different areas of Au foils (left, middle, right) was very similar and MoSe<sub>2</sub> domains distribute on the whole Au surface uniformly.

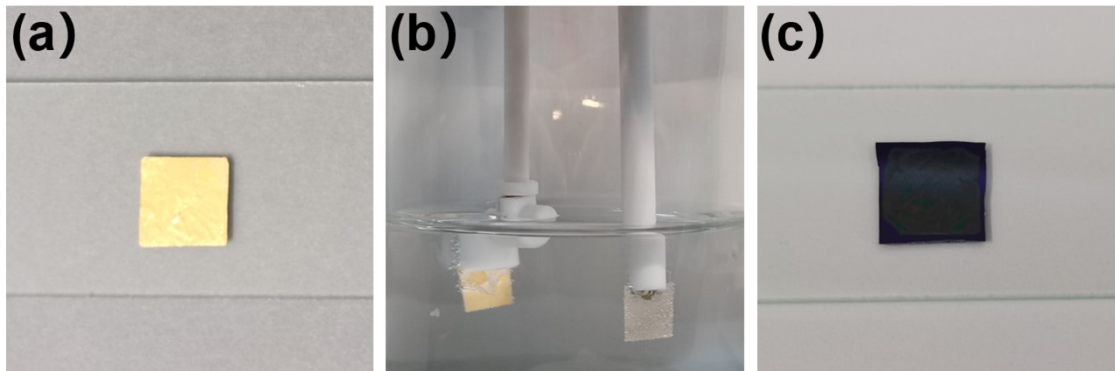


**Figure S5.** Schematic diagram of the electrochemical bubbling method for transferring MoSe<sub>2</sub> single crystals and their films. Photographs of (a) MoSe<sub>2</sub>/Au after spin-coated with PMMA, (b) the electrolysis process and (c) PMMA/MoSe<sub>2</sub> transferred onto the SiO<sub>2</sub>/Si substrate.

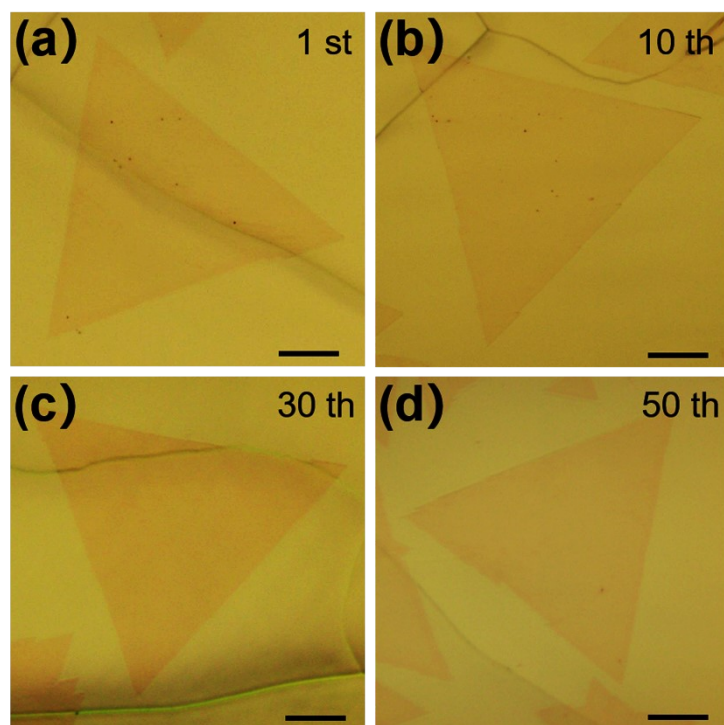


**Figure S6.** The optical images of single-crystal MoSe<sub>2</sub> domains grown on the same pre-alloyed Au foil for different times. All the MoSe<sub>2</sub> domains show the similar morphology. Before the MoSe<sub>2</sub> growth, Au foil was pre-alloyed at 1050 °C for 20 times (see Experimental, Figure 1a). Scale bar in all images is 20 μm.

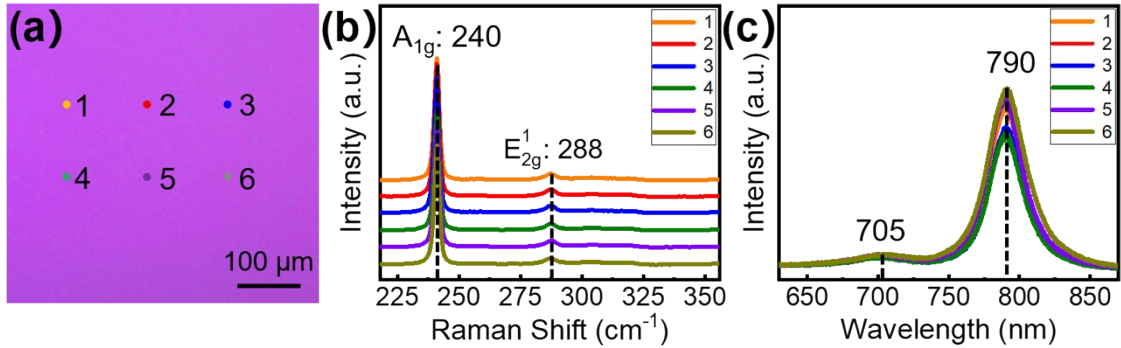


**Figure S7.** (a) Optical image of monolayer MoSe<sub>2</sub> film transferred on the SiO<sub>2</sub>/Si substrate. (b) Raman and (c) PL spectra taken from 6 positions marked with different colors in (a), showing the characteristic peaks of monolayer MoSe<sub>2</sub>. Considering that mapping a large area is very time-consuming, Raman and PL spectra were randomly taken in the MoSe<sub>2</sub> film.

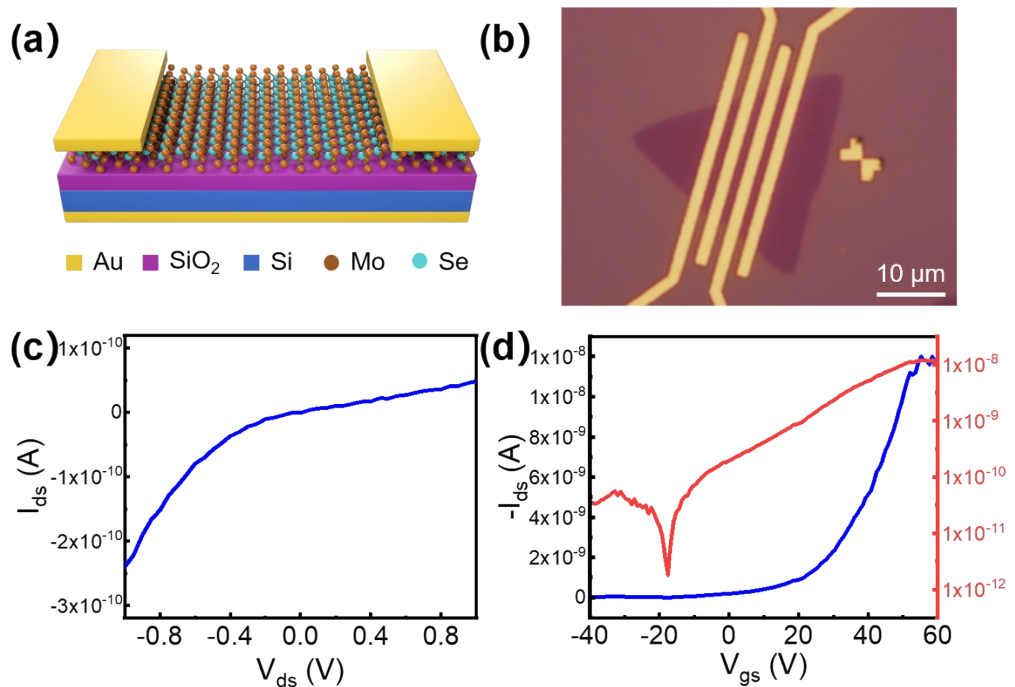


**Figure S8.** Electrical properties of monolayer single-crystal MoSe<sub>2</sub>. (a) Schematic diagram and (b) the optical image of the back-gate FET device based on the single-crystal MoSe<sub>2</sub> domain. (c) Output characteristic and (d) transfer characteristic of MoSe<sub>2</sub> FET device. The non-linear output characteristic in (c) presents a Schottky contact between the MoSe<sub>2</sub> and Au electrodes which may be caused by the inevitable contaminations during the fabrication of devices. The transfer characteristic in (d) indicates that as-grown MoSe<sub>2</sub> is a typical n-type semiconductor. The carrier mobility and ON/OFF ratio evaluated under V<sub>ds</sub> of 0.1 V from (d) is 11.6 cm<sup>2</sup> V<sup>-1</sup> s<sup>-1</sup> and ~10<sup>3</sup>, respectively.

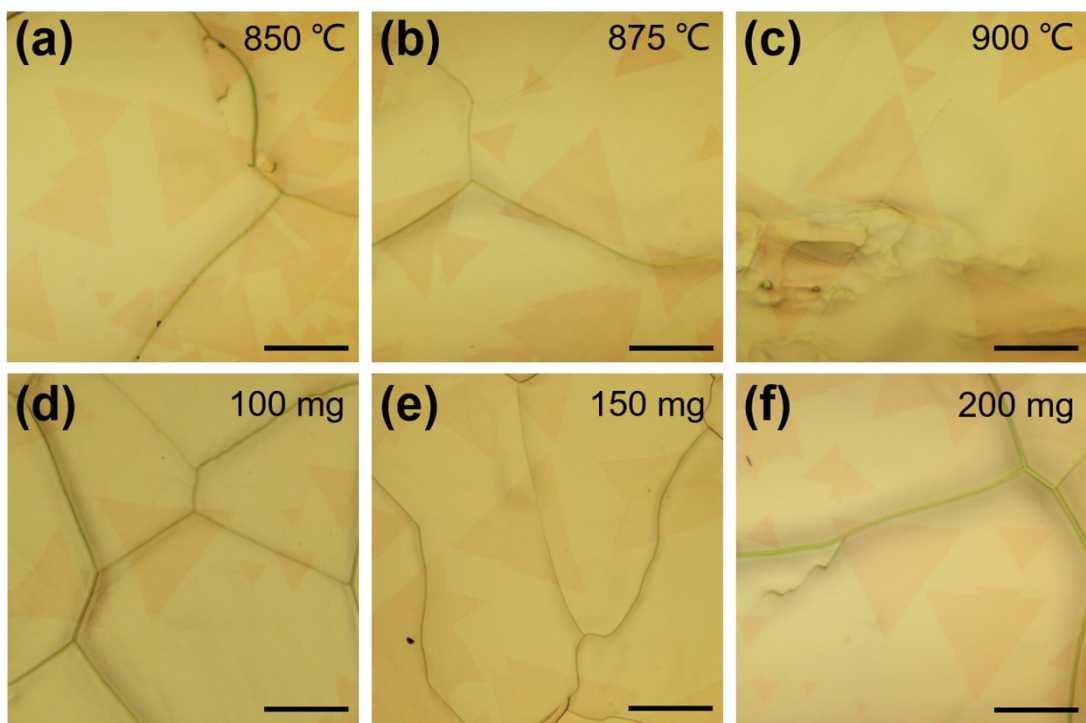


**Figure S9.** Optical images of MoSe<sub>2</sub> grown on the original Au foils under (a-c) different growth temperature and (d-f) different Se content. Scale bar in all images is 50  $\mu\text{m}$ .

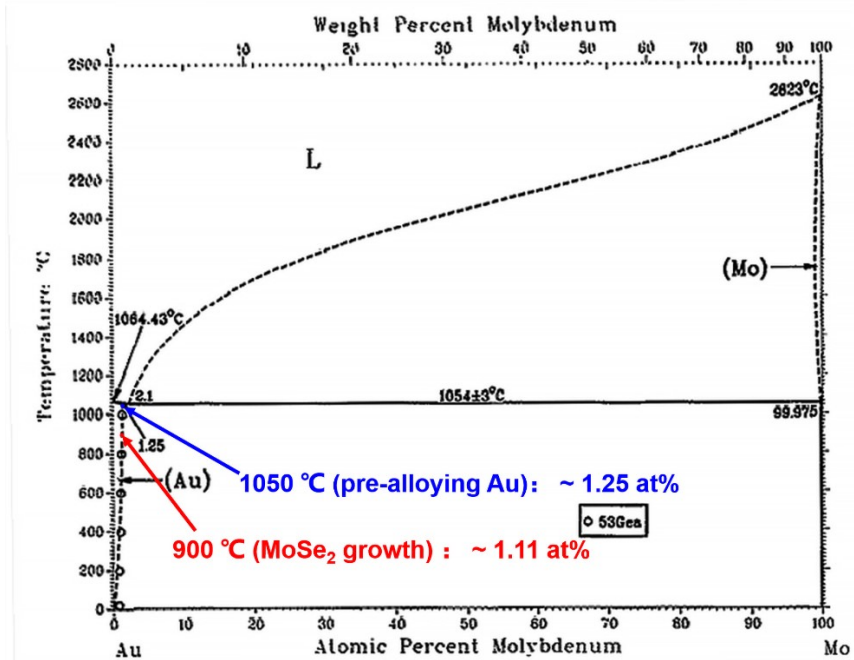


**Figure S10.** Au-Mo phase diagram.<sup>41</sup>

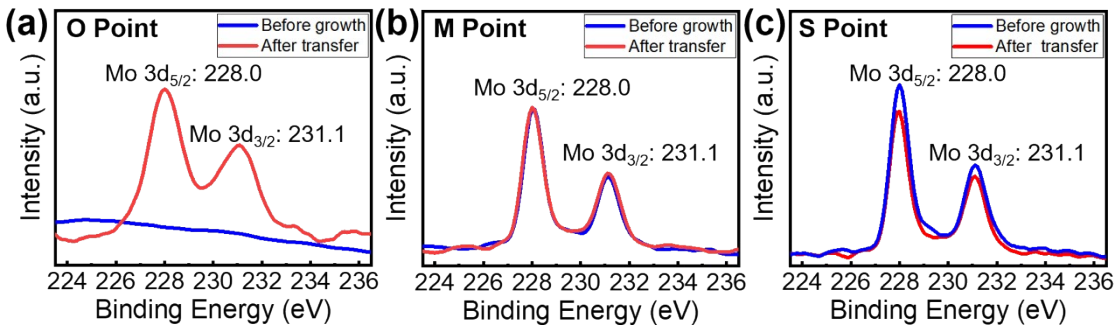


**Figure S11.** XPS spectra collected on the Au foils before and after MoSe<sub>2</sub> growth (Then MoSe<sub>2</sub> were totally transferred from Au foils). (a) At O Point, Mo content in Au increases after MoSe<sub>2</sub> growth, due to the formation of Au-Mo alloys along with the MoSe<sub>2</sub> growth on the pristine Au. (b) At M Point, the Mo content in the pre-alloyed Au remains unchanged because Mo was saturated at the MoSe<sub>2</sub> growth temperature (900 °C). (c) At S Point, the Mo content in the pre-alloyed Au is oversaturated at 900 °C. The excess Mo atoms diffuse onto the Au surface, so that the Mo content in pre-alloyed Au slightly decreases after MoSe<sub>2</sub> growth.

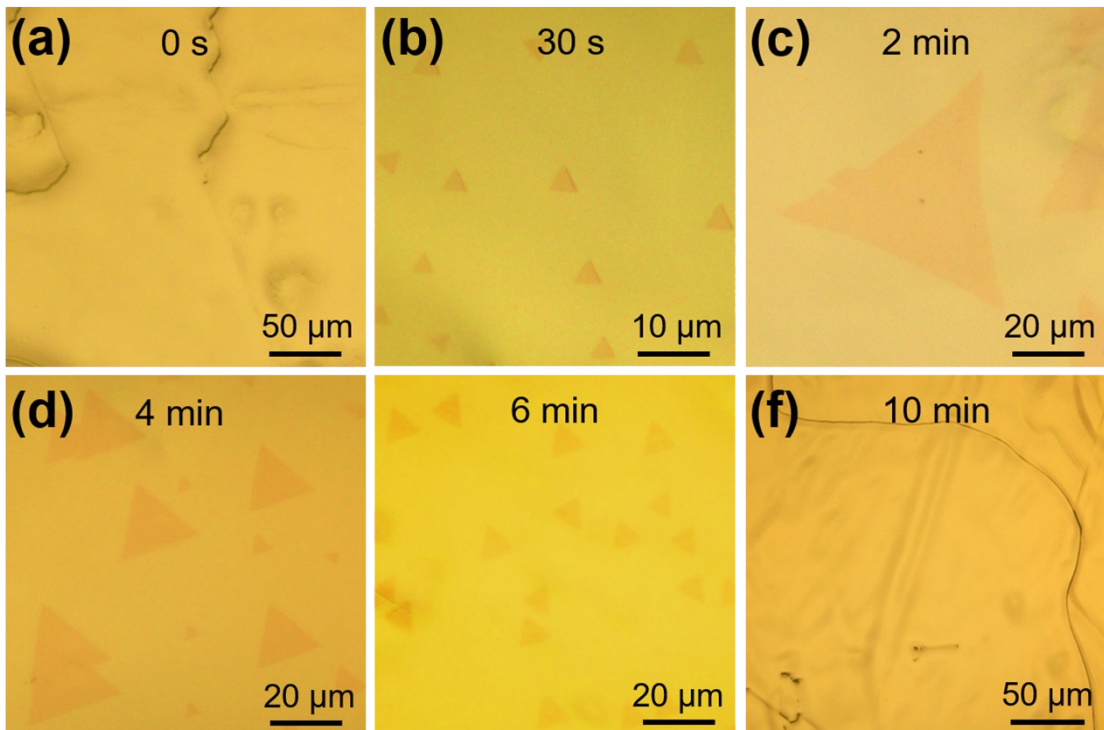


**Figure S12.** Optical images of MoSe<sub>2</sub> single crystals synthesized on pre-alloyed Au foils without MoO<sub>3</sub> precursor supply. The Au foil has been pre-alloyed for 25 times (see Experimental). The growth time in (a-f) varied from 0 to 12 min while keeping all the other parameters constant. We can see that the largest domains can be obtained within 2 min. The Mo content in the pre-alloyed Au is not enough to grow MoSe<sub>2</sub> for more than 10 min without the continuous Mo source supply.

Figure S12b and Figure 4a (the last figure) show MoSe<sub>2</sub> growth on pre-alloyed Au in 30 s without and with extra MoO<sub>3</sub> supply. Many small MoSe<sub>2</sub> nucleus (~4  $\mu\text{m}$ ) were formed without MoO<sub>3</sub> supply because of precipitation of pre-deposited Mo (Figure S12b). However, MoSe<sub>2</sub> domains can be increased 27 times larger (107  $\mu\text{m}$ ) after introducing extra MoO<sub>3</sub> supply (Figure 4a). The phenomenon proves that although the pre-deposited Mo can be act as Mo source for the MoSe<sub>2</sub> growth, it has a slight effect on promoting the grain size of MoSe<sub>2</sub>. The main Mo source for MoSe<sub>2</sub> growth come from the extra MoO<sub>3</sub> powders but not pre-deposited Mo.

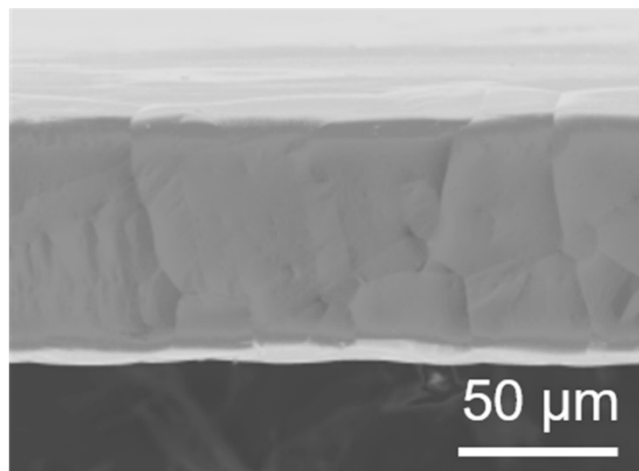


**Figure S13.** The SEM image of the cross section of pre-alloyed Au foil.

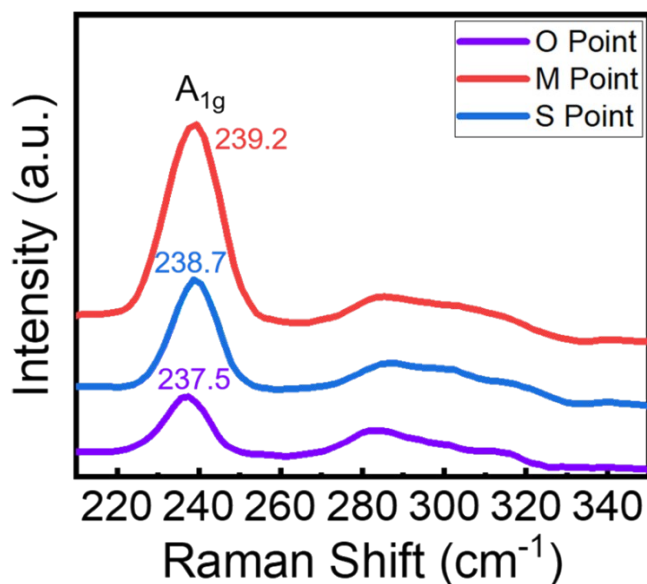


**Figure S14.** Raman spectra of MoSe<sub>2</sub> collected on Au foils with different Mo content corresponding to O Point, M Point and S Point in Figure 4c. The  $A_{1g}$  peaks at M and S Point have a blue shift than that at O Point, indicating a relative weak interaction between MoSe<sub>2</sub> and the pre-alloyed Au.

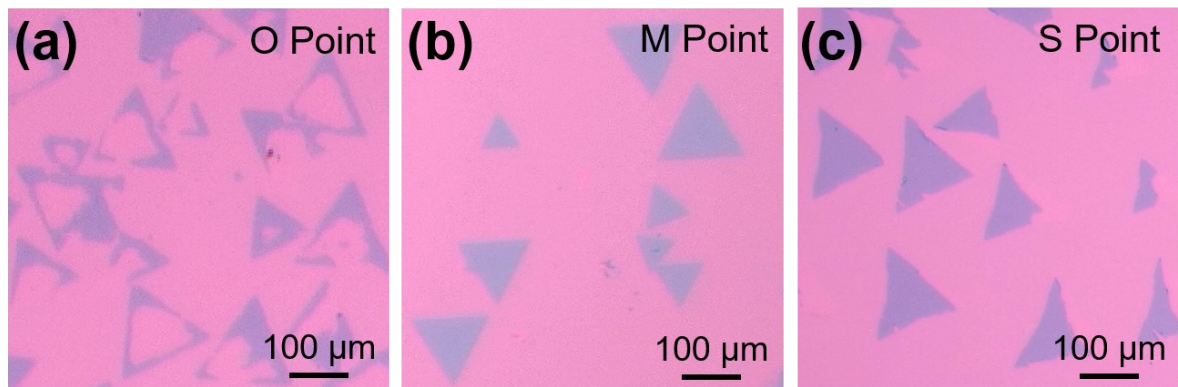


**Figure S15.** Optical images of MoSe<sub>2</sub> domains transferred from Au foils onto SiO<sub>2</sub>/Si substrates. MoSe<sub>2</sub> domains were obtained on (a) the original Au without pre-alloying (O Point), the pre-alloyed Au at (b) M Point and (c) S Point. MoSe<sub>2</sub> domains were seriously damaged in (a), while the whole triangle was completely transferred in (b).

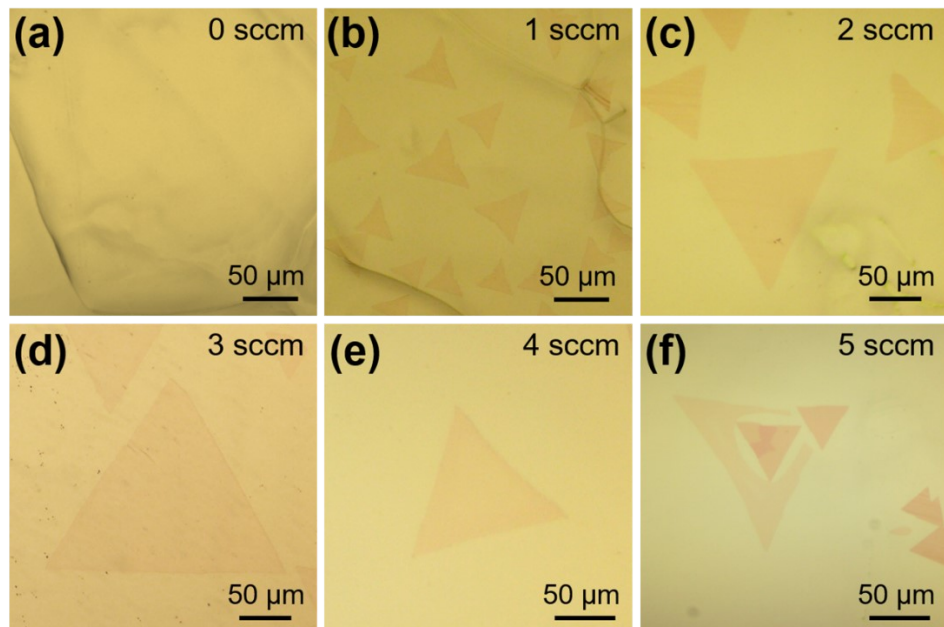


**Figure S16.** Optical images of MoSe<sub>2</sub> grown on pre-alloyed Au foils with different H<sub>2</sub> flow rate. Before the MoSe<sub>2</sub> growth, Au foils were pre-alloyed at 1050 °C for 5 times. Except for changing the H<sub>2</sub> flow rate, we kept all the other CVD parameters constant to eliminate the uncertain factors.

The grain size of monolayer MoSe<sub>2</sub> single crystals increases along with the H<sub>2</sub> concentration increasing from 0 to 3 sccm. Submillimeter-scale single-crystal MoSe<sub>2</sub> domain was achieved with a moderate H<sub>2</sub> flow of 3 sccm. Then after, grain size decreases and MoSe<sub>2</sub> multilayers appear at a higher H<sub>2</sub> flow rate.

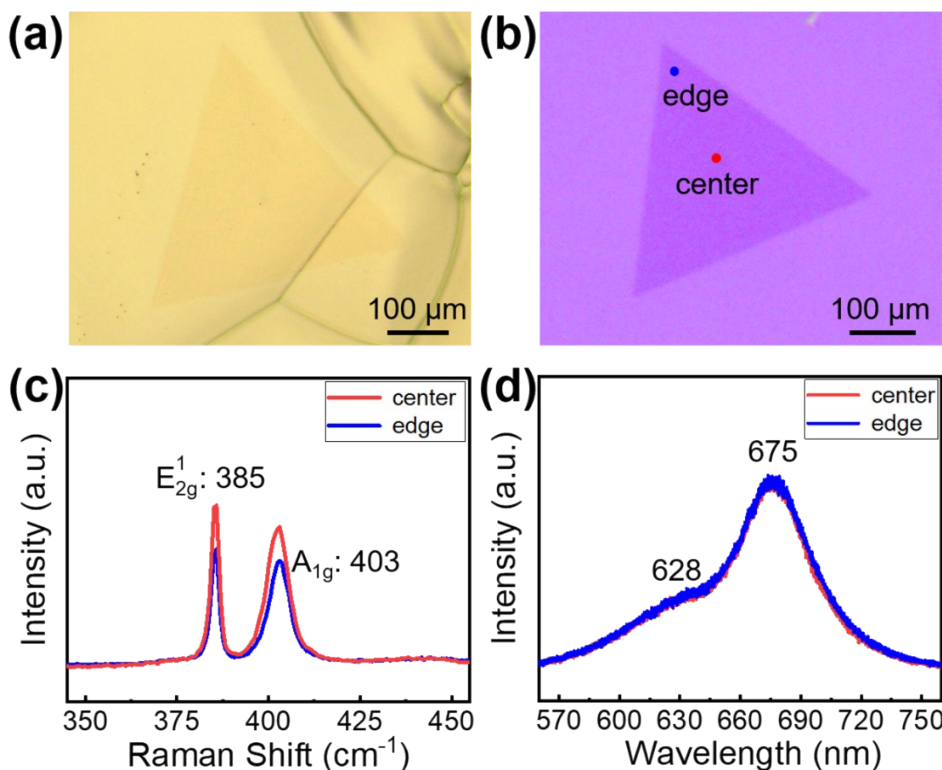


**Figure S17.** (a) An optical image of ~450  $\mu\text{m}$ -sized MoS<sub>2</sub> single crystal grown by pre-alloying CVD. (b) MoS<sub>2</sub> transferred to the SiO<sub>2</sub>/Si substrate by electrochemical bubbling method. (c) Raman and (d) PL spectra taken from the center and edge of single-crystal MoS<sub>2</sub> domain in (b).

Monolayer MoS<sub>2</sub> were obtained on pre-alloyed Au by changing the growth precursors. The 155 mg S powder (99.5 wt%) was separately heated to ~200 °C at the upstream of the pre-alloyed Au foil outside the furnace. The tube furnace was heated from room temperature to 750 °C within 20 min and then to 900 °C in 10 min under an Ar flow of 100 sccm. Then after, 3 sccm H<sub>2</sub> was turned on for 2 min.

Figure S17 shows that ~450  $\mu\text{m}$ -sized triangular MoS<sub>2</sub> was synthesized within 2 min, with a growth rate of ~3.75  $\mu\text{m s}^{-1}$ . Obviously, the value is much lower than the growth rate of MoSe<sub>2</sub> (~18.7  $\mu\text{m s}^{-1}$ ). Although the growth mechanism is similar, the growth dynamics are different between MoS<sub>2</sub> and MoSe<sub>2</sub>. In our previous reports,<sup>13</sup> we have demonstrated that S<sub>2</sub> dimer dissociate into S atoms firstly and then S atoms diffuse to form WS<sub>2</sub>. Such two processes need to overcome 0.22 eV barriers for S<sub>2</sub> dissociation and 0.58 eV barriers for S atom diffusion. By contrast, there exists only one process with a relatively smaller energy barrier (0.27 eV) for Se atoms diffusion to form WSe<sub>2</sub>.<sup>20</sup> Therefore, the growth rate of MoSe<sub>2</sub> is higher than MoS<sub>2</sub>.

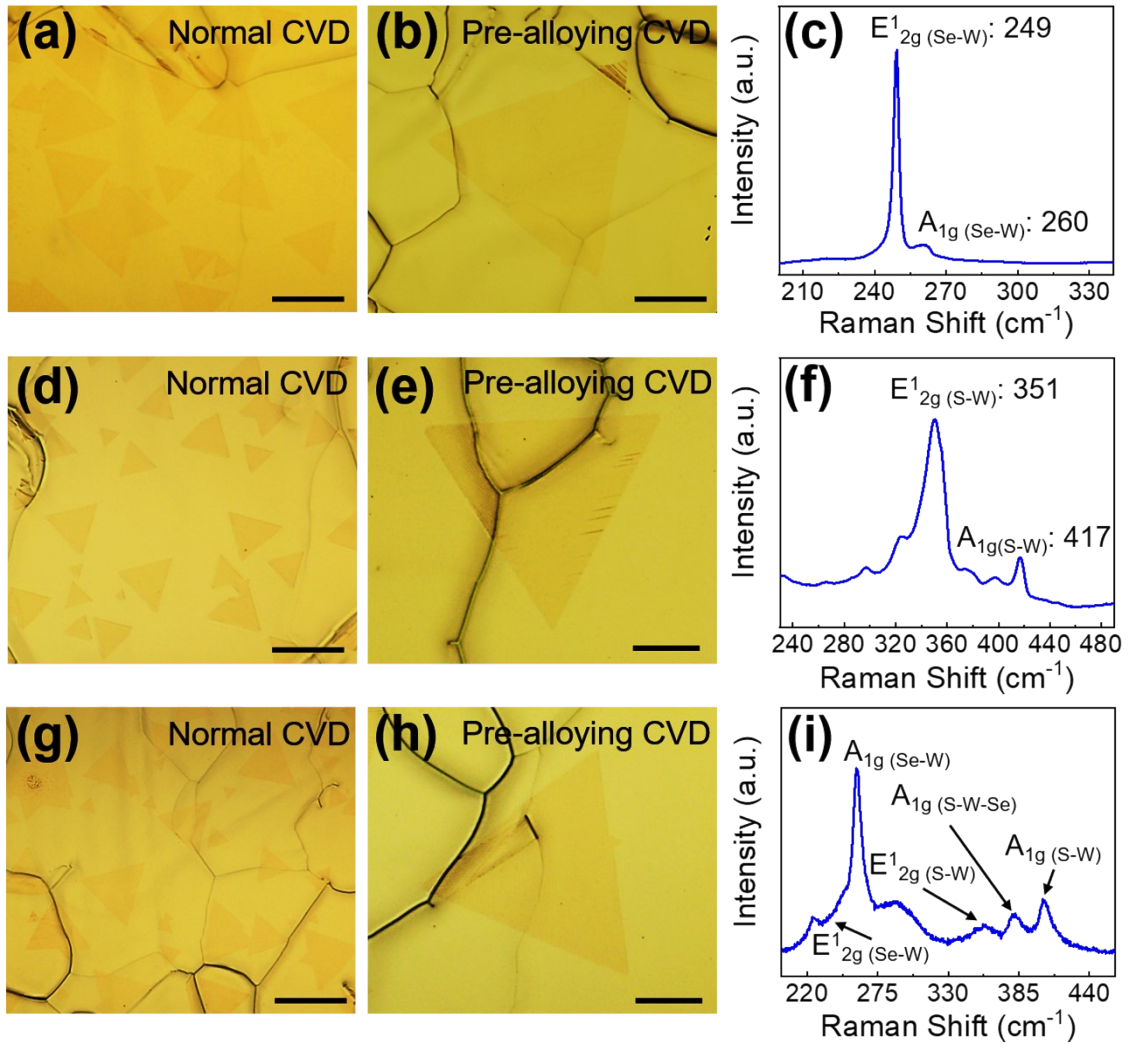


**Figure S18.** Comparison of (a-c)  $\text{WSe}_2$ , (d-f)  $\text{WS}_2$  and (g-i)  $\text{WS}_{2x}\text{Se}_{2(1-x)}$  obtained by normal and pre-alloying CVD. Figure c, f and i are the corresponding Raman spectra. Au foils were pre-alloyed at  $1050^\circ\text{C}$  for 9 times. All scale bars are  $100 \mu\text{m}$ .  $\text{WSe}_2$  was grown at  $900^\circ\text{C}$  for 2 min with an Ar and  $\text{H}_2$  flow of 100 and 3 sccm.  $\text{WS}_2$  was grown at  $850^\circ\text{C}$  for 5 min with an Ar and  $\text{H}_2$  flow of 100 and 2 sccm.  $\text{WS}_{2x}\text{Se}_{2(1-x)}$  was obtained at  $875^\circ\text{C}$  for 5 min with an Ar and  $\text{H}_2$  flow of 120 and 3 sccm. The samples obtained by pre-alloying CVD have much lower nucleation density and larger grain size.

**Table S1.** Comparison of growth method, grain size of single-crystal TMDs.

Material	Substrate	Temperature (°C)	Time	Size	Rate (μm/s)	Property	References
MoS <sub>2</sub>	SiO <sub>2</sub> /Si	700	5 min	120 μm	0.40	—	1
	Sapphire	850	10 min	350 μm	0.58	$\mu=90 \text{ cm}^2 \text{ V}^{-1} \text{ s}^{-1}$ ON/OFF 10 <sup>7</sup>	2
	SiO <sub>2</sub> /Si	850	10 min	305 μm	0.51	$\mu=28 \text{ cm}^2 \text{ V}^{-1} \text{ s}^{-1}$ ON/OFF 10 <sup>6</sup>	3
	SiO <sub>2</sub> /Si	800	5 min	500 μm	1.67	—	4
	Sapphire	775	10 min	170 μm	0.28	$\mu=3 \text{ cm}^2 \text{ V}^{-1} \text{ s}^{-1}$	5
	Anyone	750	10 min	200 μm	0.33	$\mu=90 \text{ cm}^2 \text{ V}^{-1} \text{ s}^{-1}$ ON/OFF 10 <sup>7</sup>	6
	SiO <sub>2</sub> /Si	770	15 min	500 μm	0.56	$\mu=48.7 \text{ cm}^2 \text{ V}^{-1} \text{ s}^{-1}$ ON/OFF 10 <sup>7</sup>	7
	Au foil	680	60 min	50 μm	0.01	Tafel slope: 61 mV dec <sup>-1</sup> $J: 38.1 \mu\text{A cm}^{-2}$	8
	Au foil	680	60 min	81 μm	0.02	—	9

	Au foil	680	60 min	115 $\mu\text{m}$	0.03	—	10
	<b>Au foil</b>	<b>900</b>	<b>2 min</b>	<b>450 <math>\mu\text{m}</math></b>	<b>3.75</b>	—	<b>Our work</b>
WS <sub>2</sub>	SiO <sub>2</sub> /Si	750	5 min	178 $\mu\text{m}$	0.59	—	11
	Sapphire	900	60 min	135 $\mu\text{m}$	0.04	$\mu=4.1 \text{ cm}^2 \text{ V}^{-1} \text{ s}^{-1}$	12
	Au foil	800	4 h	600 $\mu\text{m}$	0.04	$\mu=2 \text{ cm}^2 \text{ V}^{-1} \text{ s}^{-1}$ ON/OFF 10 <sup>7</sup>	13
	Au foil	935	15 min	420 $\mu\text{m}$	0.47	$\mu=20 \text{ cm}^2 \text{ V}^{-1} \text{ s}^{-1}$ ON/OFF 10 <sup>8</sup>	14
	SiO <sub>2</sub> /Si	900	10 min	250 $\mu\text{m}$	0.42	$\mu=32.3 \text{ cm}^2 \text{ V}^{-1} \text{ s}^{-1}$	15
	SiO <sub>2</sub> /Si	950	5 min	360 $\mu\text{m}$	1.20	—	4
	SiO <sub>2</sub> /Si	1070	15 min	256 $\mu\text{m}$	0.28	$\mu=2.2 \text{ cm}^2 \text{ V}^{-1} \text{ s}^{-1}$	16
WSe <sub>2</sub>	Sapphire	850	15 min	50 $\mu\text{m}$	0.06	$\mu=90 \text{ cm}^2 \text{ V}^{-1} \text{ s}^{-1}$	17
	SiO <sub>2</sub> /Si	720	30 min	168 $\mu\text{m}$	0.09	$\mu=100 \text{ cm}^2 \text{ V}^{-1} \text{ s}^{-1}$ ON/OFF 10 <sup>7</sup>	18
	SiO <sub>2</sub> /Si	900	20 min	800 $\mu\text{m}$	0.67	—	19
	Au foil	950	30 s	780 $\mu\text{m}$	26.00	$\mu=143 \text{ cm}^2 \text{ V}^{-1} \text{ s}^{-1}$	20

					ON/OFF $9 \times 10^6$	
	SiO <sub>2</sub> /Si	1050	10 min	570 $\mu\text{m}$	0.95	$\mu < 0.1 \text{ cm}^2 \text{ V}^{-1} \text{ s}^{-1}$
	Quartz	850	20 min	100 $\mu\text{m}$	0.08	PL QY ~60%
	hBN	800	20 min	380 $\mu\text{m}$	0.32	$\mu = 4.2 \text{ cm}^2 \text{ V}^{-1} \text{ s}^{-1}$
MoSe <sub>2</sub>	SiO <sub>2</sub> /Si	750	10 min	30 $\mu\text{m}$	0.05	—
	SiO <sub>2</sub> /Si	820	15 min	40 $\mu\text{m}$	0.04	R=13 mA W <sup>-1</sup>
	SiO <sub>2</sub> /Si	750	20 min	135 $\mu\text{m}$	0.11	$\mu = 50 \text{ cm}^2 \text{ V}^{-1} \text{ s}^{-1}$ ON/OFF > $10^6$
	SiO <sub>2</sub> /Si	750	10 min	50 $\mu\text{m}$	0.08	—
	SiO <sub>2</sub> /Si	750	20 min	1.3 mm	1.08	$\mu = 42 \text{ cm}^2 \text{ V}^{-1} \text{ s}^{-1}$ ON/OFF $10^6$
	Molten glass	1050	5 min	2.5 mm	8.33	$\mu = 95 \text{ cm}^2 \text{ V}^{-1} \text{ s}^{-1}$ ON/OFF > $10^7$
	SiO <sub>2</sub> /Si Quartz	750	20 min	100 $\mu\text{m}$	0.08	—
	SiO <sub>2</sub> /Si	730	15 min	195 $\mu\text{m}$	0.22	—
	SiO <sub>2</sub> /Si	730	3 min	135 $\mu\text{m}$	0.75	—
	Au foil	900	30 s	560 $\mu\text{m}$	18.67	$\mu = 11.6 \text{ cm}^2 \text{ V}^{-1} \text{ s}^{-1}$
						Our work

**Table S2.** Comparison of single-crystal TMDs grown on Au.

Materials	Temperature (°C)	Time	Size	Rate (μm/s)	Property	References
ReSe <sub>2</sub>	750	15 min	Monolayer parallelogram: 20 μm	0.02	—	32
	750	15 min	—	—	—	33
	750	30 min	Monolayer: 30 μm	0.02	—	34
ReS <sub>2</sub>	800	5 min	—	—	$\mu=2.3 \text{ cm}^2 \text{ V}^{-1} \text{ s}^{-1}$ $R=178.75 \text{ A W}^{-1}$	35
PtTe <sub>2</sub>	800	10 min	5.6-50 nm Rectangular: 200 μm; triangular: 30 μm	Rectangular: 0.33 Triangular: 0.05	$R=250 \text{ mA W}^{-1}$	36
PtSe <sub>2</sub>	850	20 min	Irregular: 245 μm	0.20	Tafel slope: ~33 mV dec <sup>-1</sup> $J: \sim 215 \mu\text{A cm}^{-2}$	37
TaSe <sub>2</sub>	930	5-25 min	Different thickness: 5-20 μm	—	—	38
TaS <sub>2</sub>	750	10 min	Different thickness: 20 μm	0.03	Tafel slope: 33-42 mV dec <sup>-1</sup> $J: 100-179 \mu\text{A cm}^{-2}$	39
WS <sub>2</sub>	800	4 h	600 μm	0.04	$\mu=2 \text{ cm}^2 \text{ V}^{-1} \text{ s}^{-1}$ ON/OFF 10 <sup>7</sup>	13

	935	15 min	420 $\mu\text{m}$	0.47	$\mu=20 \text{ cm}^2 \text{ V}^{-1} \text{ s}^{-1}$ ON/OFF $10^8$	14
WSe <sub>2</sub>	950	30 s	780 $\mu\text{m}$	26.00	$\mu=143 \text{ cm}^2 \text{ V}^{-1} \text{ s}^{-1}$ ON/OFF $9*10^6$	20
MoS <sub>2</sub>	680	60 min	50 $\mu\text{m}$	0.01	Tafel slope: 61 mV $\text{dec}^{-1}$ J: 38.1 $\mu\text{A cm}^{-2}$	8
	680	60 min	81 $\mu\text{m}$	0.02	—	9
	680	60 min	115 $\mu\text{m}$	0.03	—	10
	720	8 min	film	—	$\mu=11.2 \text{ cm}^2 \text{ V}^{-1} \text{ s}^{-1}$ ON/OFF $7.7*10^5$	40
	<b>900</b>	<b>2 min</b>	<b>450 <math>\mu\text{m}</math></b>	<b>3.75</b>	—	<b>Our work</b>
MoSe <sub>2</sub>	<b>900</b>	<b>30 s</b>	<b>560 <math>\mu\text{m}</math></b>	<b>18.67</b>	<b><math>\mu=11.6 \text{ cm}^2 \text{ V}^{-1} \text{ s}^{-1}</math></b>	<b>Our work</b>

## References

- 1 A. M. van der Zande, P. Y. Huang, D. A. Chenet, T. C. Berkelbach, Y. You, G. H. Lee, T. F. Heinz, D. R. Reichman, D. A. Muller and J. C. Hone, *Nat. Mater.*, 2013, **12**, 554.
- 2 W. Chen, J. Zhao, J. Zhang, L. Gu, Z. Yang, X. Li, H. Yu, X. Zhu, R. Yang, D. Shi, X. Lin, J. Guo, X. Bai and G. Zhang, *J. Am. Chem. Soc.*, 2015, **137**, 15632.
- 3 J. Chen, W. Tang, B. Tian, B. Liu, X. Zhao, Y. Liu, T. Ren, W. Liu, D. Geng, H. Y. Jeong, H. S. Shin, W. Zhou and K. P. Loh, *Adv. Sci.*, 2016, **3**, 1500033.
- 4 J. Lee, S. Pak, P. Giraud, Y. W Lee, Y. Cho, J. Hong, A. R. Jang, H. S. Chung, W. K. Hong, H. Y. Jeong, H. S. Shin, L. G. Occhipinti, S. M. Morris, S. Cha, J. I. Sohn and J. M. Kim, *Adv. Mater.*, 2017, **29**, 1702206.
- 5 Y. F. Lim, K. Priyadarshi, F. Bussolotti, P. K. Gogoi, X. Cui, M. Yang, J. Pan, S. W. Tong, S. Wang, S. J. Pennycook, K. E. J. Goh, A. T. S. Wee, S. L. Wong and D. Chi, *ACS Nano*, 2018, **12**, 1339.
- 6 J. Zhu, H. Xu, G. Zou, W. Zhang, R. Chai, J. Choi, J. Wu, H. Liu, G. Shen and H. Fan, *J. Am. Chem. Soc.*, 2019, **141**, 5392.
- 7 X. Li, E. Kahn, G. Chen, X. Sang, J. Lei, D. Passarello, A. D. Oyedele, D. Zakhidov, K. W. Chen, Y. X. Chen, S. H. Hsieh, K. Fujisawa, R. R. Unocic, K. Xiao, A. Salleo, M. F. Toney, C. H. Chen, E. Kaxiras, M. Terrones, B. I. Yakobson and A. R. Harutyunyan, *ACS Nano*, 2020, **14**, 6570.
- 8 J. Shi, D. Ma, G. F. Han, Y. Zhang, Q. Ji, T. Gao, J. Sun, X. Song, C. Li, Y. Zhang, X. Y. Lang, Y. Zhang and Z. Liu, *ACS Nano*, 2014, **8**, 10196.
- 9 J. Shi, Y. Yang, Y. Zhang, D. Ma, W. Wei, Q. Ji, Y. Zhang, X. Song, T. Gao, C. Li, X. Bao, Z. Liu, Q. Fu and Y. Zhang, *Adv. Funct. Mater.*, 2015, **25**, 842.
- 10 J. Shi, X. Zhang, D. Ma, J. Zhu, Y. Zhang, Z. Guo, Y. Yao, Q. Ji, X. Song, Y. Zhang, C. Li, Z. Liu, W. Zhu and Y. Zhang, *ACS Nano*, 2015, **9**, 4017.
- 11 C. Cong, J. Shang, X. Wu, B. Cao, N. Peimyoo, C. Qiu, L. Sun and T. Yu, *Adv. Opt. Mater.*, 2014, **2**, 131.
- 12 Q. Xu, Y. Zhang, S. Lin, C. Zheng, Y. L. Zhong, X. Xia, Z. Li, P. J. Sophia, M. S. Fuhrer, Y. B. Cheng and Q. Bao, *ACS Nano*, 2015, **9**, 6178.
- 13 Y. Gao, Z. Liu, D. M. Sun, L. Huang, L. P. Ma, L. C. Yin, T. Ma, Z. Zhang, X. L. Ma, L. M. Peng, H. M. Cheng and W. Ren, *Nat. Commun.*, 2015, **6**, 8569.

- 14 S. J. Yun, S. H. Chae, H. Kim, J. C. Park, J. H. Park, G. H. Han, J. S. Lee, S. M. Kim, H. M. Oh, J. Seok, M. S. Jeong, K. K. Kim and Y. H. Lee, *ACS Nano*, 2015, **9**, 5510.
- 15 Y. Yue, J. Chen, Y. Zhang, S. Ding, F. Zhao, Y. Wang, D. Zhang, R. Li, H. Dong, W. Hu, Y. Feng and W. Feng, *ACS Appl. Mater. Interfaces*, 2018, **10**, 22435.
- 16 L. Dong, Y. Wang, J. Sun, C. Pan, Q. Zhang, L. Gu, B. Wan, C. Song, F. Pan, C. Wang, Z. Tang and J. Zhang, *2D Mater.*, 2019, **6**, 015007.
- 17 J. K. Huang, J. Pu, C. L. Hsu, M. H. Chiu, Z. Y. Juang, Y. H. Chang, W. H. Chang, Y. Iwasa, T. Takenobu and L. J. Li, *ACS Nano*, 2014, **8**, 923.
- 18 J. Chen, B. Liu, Y. Liu, W. Tang, C. T. Nai, L. Li, J. Zheng, L. Gao, Y. Zheng, H. S. Shin, H. Y. Jeong and K. P. Loh, *Adv. Mater.*, 2015, **27**, 6722.
- 19 Y. J. Gong, G. Ye, S. Lei, G. Shi, Y. He, J. Lin, X. Zhang, R. Vajtai, S. T. Pantelides, W. Zhou, B. Li and P. M. Ajayan, *Adv. Funct. Mater.*, 2016, **26**, 2009.
- 20 Y. Gao, Y. L. Hong, L. C. Yin, Z. Wu, Z. Yang, M. L. Chen, Z. Liu, T. Ma, D. M. Sun, Z. Ni, X. L. Ma, H. M. Cheng and W. Ren, *Adv. Mater.*, 2017, **29**, 1700990.
- 21 Q. Feng, M. Zhu, Y. Zhao, H. Liu, M. Li, J. Zheng, H. Xu and Y. Jiang, *Nanotechnology*, 2018, **30**, 034001.
- 22 H. Kim, G. H. Ahn, J. Cho, M. Amani, J. P. Mastandrea, C. K. Groschner, D. H. Lien, Y. Zhao, J. W. Ager III, M. C. Scott, D. C. Chrzan, A. Javey, *Sci. Adv.*, 2019, **5**, 2375.
- 23 X. Zhang, F. Zhang, Y. Wang, D. S. Schulman, T. Zhang, A. Bansal, N. Alem, S. Das, V. H. Crespi, M. Terrones and J. M. Redwing, *ACS Nano* 2019, **13**, 3341.
- 24 J. C. Shaw, H. Zhou, Y. Chen, N. O. Weiss, Y. Liu, Y. Huang and X. Duan, *Nano Res.*, 2014, **7**, 511.
- 25 J. Xia, X. Huang, L. Z. Liu, M. Wang, L. Wang, B. Huang, D. D. Zhu, J. J. Li, C. Z. Gu and X. M. Meng, *Nanoscale*, 2014, **6**, 8949.
- 26 X. Wang, Y. Gong, G. Shi, W. L. Chow, K. Keyshar, G. Ye, R. Vajtai, J. Lou, Z. Liu, E. Ringe, B. K. Tay and P. M. Ajayan, *ACS Nano*, 2014, **8**, 5125.
- 27 B. Li, Y. Gong, Z. Hu, G. Brunetto, Y. Yang, G. Ye, Z. Zhang, S. Lei, Z. Jin, E. Bianco, X. Zhang, W. Wang, J. Lou, D. S. Galvão, M. Tang, B. I. Yakobson, R. Vajtai and P. M. Ajayan, *Angew. Chem. Int. Ed.*, 2016, **55**, 10656.
- 28 J. Chen, X. Zhao, S. J. R. Tan, H. Xu, B. Wu, B. Liu, D. Fu, W. Fu, D. Geng, Y. Liu, W. Liu, W. Tang, L. Li, W. Zhou, T. C. Sum and K. P. Loh, *J. Am. Chem. Soc.*, 2017, **139**, 1073.

- 29 I. Bilgin, A. S. Raeliarijaona, M. C. Lucking, S. C. Hodge, A. D. Mohite, A. de Luna Bugallo, H. Terrones and S. Kar, *ACS Nano*, 2018, **12**, 740.
- 30 T. Chen, G. Hao, G. Wang, B. Li, L. Kou, H. Yang, X. Zheng and J. Zhong, *2D Mater.*, 2019, **6**, 025002.
- 31 R. Shi, P. He, X. Cai, Z. Zhang, Wang, W. J. Wang, X. Feng, Z. Wu, A. Amini, N. Wang and C. Cheng, *ACS Nano*, 2020, **14**, 7593.
- 32 S. Jiang, M. Hong, W. Wei, L. Zhao, N. Zhang, Z. Zhang, P. Yang, N. Gao, X. Zhou, C. Xie, J. Shi, Y. Huan, L. Tong, J. Zhao, Q. Zhang, Q. Fu and Y. Zhang, *Commun. Chem.*, 2018, **1**, 17.
- 33 M. Hong, X. Zhou, N. Gao, S. Jiang, C. Xie, L. Zhao, Y. Gao, Z. Zhang, P. Yang, Y. Shi, Q. Zhang, Z. Liu, J. Zhao and Y. Zhang, *ACS Nano*, 2018, **12**, 10095.
- 34 S. Jiang, L. Zhao, Y. Shi, C. Y. Xie, N. Zhang, Z. Zhang, Y. Huan, P. Yang, M. Hong, X. Zhou, J. Shi, Q. Zhang and Y. Zhang, *Nanotechnology*, 2018, **29**, 204003.
- 35 X. Li, X. Dai, D. Tang, X. Wang, J. Hong, C. Chen, Y. Yang, J. Lu, J. Zhu, Z. Lei, K. Suenaga, F. Ding and H. Xu, *Adv. Funct. Mater.*, 2021, **31**, 2102138.
- 36 Y. Yang, K. Zhang, L. Zhang, G. Hong, C. Chen, H. Jing, J. Lu, P. Wang, X. Chen, L. Wang and H. Xu, *InfoMat*, 2021, **3**, 705.
- 37 J. Shi, Y. Huan, M. Hong, R. Xu, P. Yang, Z. Zhang, X. Zou and Y. Zhang, *ACS Nano*, 2019, **13**, 8442.
- 38 J. Shi, X. Chen, L. Zhao, Y. Gong, M. Hong, Y. Huan, Z. Zhang, P. Yang, Y. Li, Q. Zhang, Q. Zhang, L. Gu, H. Chen, J. Wang, S. Deng, N. Xu and Y. F. Zhang, *Adv. Mater.*, 2018, **30**, 1804616.
- 39 J. Shi, X. Wang, S. Zhang, L. Xiao, Y. Huan, Gong, Y. Z. Zhang, Y. Li, X. Zhou, M. Hong, Q. Fang, Q. Zhang, X. Liu, L. Gu, Z. Liu and Y. Zhang, *Nat. Commun.*, 2017, **8**, 958.
- 40 P. Yang, S. Zhang, S. Pan, B. Tang, Y. Liang, X. Zhao, Z. Zhang, J. Shi, Y. Huan, Y. Shi, S. J. Pennycook, Z. Ren, G. Zhang, Q. Chen, X. Zou, Z. Liu and Y. Zhang, *ACS Nano*, 2020, **14**, 5036.
- 41 T. B. Massalski, H. Okamoto and L. Brewer, *Bull. Alloy Phase Diagrams*, 1986, **7**, 449.